

Porous MnO₂ for use in a high performance supercapacitor: replication of a 3D graphene network as a reactive template†

Cite this: *Chem. Commun.*, 2013, **49**, 11092

Received 8th September 2013,
Accepted 8th October 2013

DOI: 10.1039/c3cc46867d

www.rsc.org/chemcomm

Xiaoying Xie,^a Chen Zhang,^a Ming-Bo Wu,^b Ying Tao,^a Wei Lv^{ac} and Quan-Hong Yang^{*ac}

Graphene oxide hydrogel is used as a reactive template to prepare nanoporous materials with a 3D microstructure. The as-prepared porous MnO₂ shows a capacitance retention of ~70.6% at a current density as high as 15 A g⁻¹, resulting from the 3D interconnected ion transport channel replicated from the graphene oxide hydrogel.

Carbon-based supercapacitors are characterized with a long cycle life and high power density.^{1,2} However, the low energy density hinders their use as the main power source in the fields of electric vehicles and industrial scale power. Hence, great efforts have been made to prepare electrode materials with high energy density. Nanostructured metal oxides, such as MnO₂, RuO₂ and NiO, storing charge through reversible redox reactions, could satisfy the requirement and deliver a higher energy density than conventional carbon materials.^{3–5} Among these materials, MnO₂ has been paid much attention due to its structural flexibility, abundant availability and environmentally friendly nature. Unfortunately, most MnO₂ materials still suffer from poor power density as other metal oxides do, because of severe structural changes during the charge and discharge process. Therefore, it is urgently needed to design and construct a MnO₂ with a structure that provides both high energy density and excellent power capability.

Minimal ion diffusion resistance and fast transport are key factors to achieve a high power density for supercapacitors.^{6,7} Many researchers have proposed that materials with a 3D porous structure are beneficial for reducing the ion diffusion

resistance and optimizing the transport kinetics, which could ensure that MnO₂ possesses both high energy density and power capability.^{2,8} To date, several approaches have been developed for the fabrication of MnO₂ with a 3D porous texture, including hydrothermal reaction,⁹ thermal decomposition,¹⁰ templating,¹¹ *etc.* The template method is one of the most effective methods to synthesize nanomaterials with controllable structure and morphology.^{12,13} However, conventional template methods have some drawbacks such as they cause etching of the template with corrosive acid or alkali, are time-consuming and require multistep procedures. The recently developed graphene oxide hydrogel^{14,15} possesses abundant hierarchical pores and a 3D porous framework providing an interconnected ion diffusion channel, and may be a promising template to synthesize nanomaterials with a 3D porous structure although no related results have been reported thus far.

In this communication, we present an example to use the graphene oxide hydrogel as a porous template to produce porous materials. A simple *in situ* method is reported to synthesize porous MnO₂ (P-MnO₂) with a 3D framework using the graphene oxide hydrogel as a reactive template, in which the 3D carbon backbone of the starting hydrogel is completely replaced by the resulting nanostructured MnO₂. The produced P-MnO₂ can be separated from the soluble reaction byproducts (K₂CO₃, KHCO₃ and the residue KMnO₄) by a simple centrifugation. The as-prepared P-MnO₂ delivers a specific capacitance of up to 218 F g⁻¹ at 0.1 A g⁻¹ in a 1 M Na₂SO₄ aqueous electrolyte. More promisingly, a specific capacitance of up to 154 F g⁻¹ can be obtained at a current density as high as 15 A g⁻¹, and its capacitance retention ratio is ~70.6%.

It has been proved that carbon atoms in a graphene platelet may react with Mn⁷⁺ to form CO₂ and Mn⁴⁺, and graphene was used as a starting reagent to produce 2D MnO₂ nanolamellas.¹⁶ As shown in Fig. 1a, the graphene oxide hydrogel with a 3D framework prepared by a one-step hydrothermal method is immersed in the KMnO₄ solution and provides abundant carbon atoms that react with KMnO₄. Due to the thin-layered structure, almost all the carbon atoms in the graphene oxide hydrogel are reactive and replicated to form the produced

^a Key Laboratory for Green Chemical Technology of Ministry of Education, School of Chemical Engineering and Technology, Tianjin University, Tianjin, China.
E-mail: qhyangcn@tju.edu.cn; Fax: +86-22-2740-1097; Tel: +86-22-2740-1097

^b State Key Laboratory of Heavy Oil Processing, China University of Petroleum, Qingdao, China

^c Engineering Laboratory for Functionalized Carbon Materials, Graduate School at Shenzhen, Tsinghua University, Shenzhen, China.

E-mail: yang.quanhong@sz.tsinghua.edu.cn; Fax: +86-755-2603-6133;
Tel: +86-755-2603-6133

† Electronic supplementary information (ESI) available: Experimental details and supplementary figures. See DOI: 10.1039/c3cc46867d

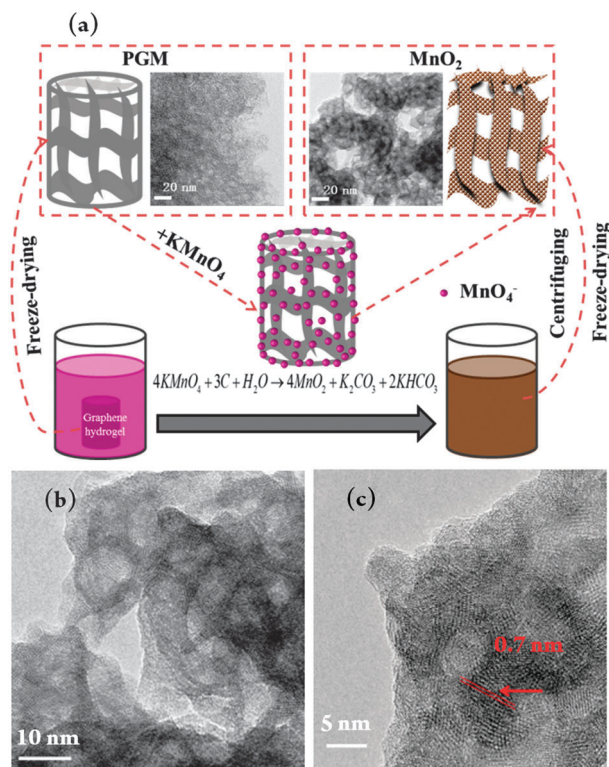


Fig. 1 (a) Schematic illustration of the formation of 3D porous MnO_2 (P- MnO_2) replicated from the graphene oxide hydrogel with a 3D framework. (b) and (c) TEM images of P- MnO_2 .

porous materials. With the replacement of carbon atoms by MnO_2 , the solution colour gradually changed from dark purple to black/brown (as schematically presented in Fig. 1a and revealed in Fig. S1, ESI[†]), indicating the transformation from MnO_4^- to MnO_2 and meanwhile the hydrogel, as a reactive template, disappeared completely when the KMnO_4 is overdosed.

TEM images (Fig. 1a and more details in Fig. 1b and c) show that the as-obtained P- MnO_2 nanoparticles with a size of *ca.* 5 nm aggregate and form a 3D porous structure that is dominated by mesopores, indicating that P- MnO_2 replicates the structure of the graphene oxide hydrogel in the nanoscale (TEM image in Fig. 1a). Note that due to the weak interaction among MnO_2 particles, P- MnO_2 hardly forms a large macroform (SEM image shown in Fig. S2b, ESI[†]) like the parent template with a hierarchical porous structure (SEM image shown in Fig. S2a, ESI[†]). The pore structure of P- MnO_2 was further characterized by nitrogen cryo-adsorption and analyzed using the Barret-Joyner-Halenda (BJH) method. As shown in Fig. 2a, P- MnO_2 possesses a typical type IV adsorption isotherm, suggesting the existence of mesopores. The BJH analysis indicates that most of the contained mesopores are in a narrow range of the pore size from 2 to 10 nm (Fig. S3c, ESI[†]). In comparison, the isotherm of the freeze-dried graphene oxide hydrogel (porous graphene-based macroform, denoted PGM) possesses mixed characteristics of types I and IV, which indicates coexistence of micropores and mesopores except for the macropores observed in a SEM (Fig. S2a, ESI[†]). That is, P- MnO_2 is free of micropores due to the thicker layer of MnO_2 . These mesopores and the 3D network of

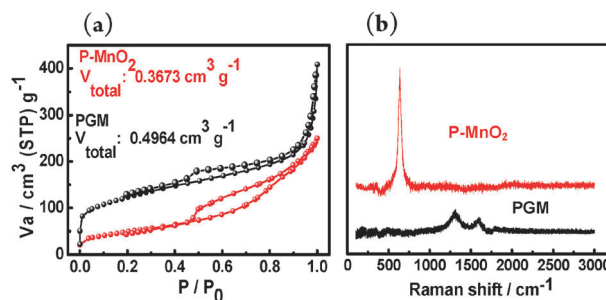


Fig. 2 (a) Nitrogen cryo-adsorption isotherms and (b) Raman spectra of P- MnO_2 and PGM that denote porous graphene macroform by freeze drying of the graphene oxide hydrogel.

P- MnO_2 could greatly facilitate ion transport and promote the bulk redox reaction in the electrode, and thus improve the rate performance. Based on the Brunauer-Emmett-Teller (BET) method, the calculated surface area of P- MnO_2 reaches a value of $145 \text{ m}^2 \text{ g}^{-1}$. Due to the porous structure, it is apparently higher than that of bulk MnO_2 ($50.3 \text{ m}^2 \text{ g}^{-1}$) and the reported graphene- MnO_2 hybrid ($95.1 \text{ m}^2 \text{ g}^{-1}$).^{16,17} The large surface area is beneficial for MnO_2 to accelerate the fast surface adsorption-desorption of the electrolyte ions on the electrode to contribute to a high specific capacitance. Note that in spite of successful replication of the 3D structure of the parent template, the specific surface area of P- MnO_2 is apparently lower than that of PGM ($435 \text{ m}^2 \text{ g}^{-1}$), which is resulted from the absence of micropores discussed above and the higher molecular mass of MnO_2 than carbon.

The replacement of carbon atoms in the 3D structure of the graphene oxide hydrogel with P- MnO_2 is further proved by Raman and X-ray photoelectron spectroscopy (XPS). In Fig. 2b, the Raman spectrum of P- MnO_2 is dominated by a sharp peak at 640 cm^{-1} , corresponding to the Mn-O vibration of the MnO_6 octahedral group.¹⁸ No D-band ($\sim 1350 \text{ cm}^{-1}$) or G band (1550 cm^{-1}), typical for the graphene oxide hydrogel, was observed, further proving the successful replication of the reactive template and the sacrifice of carbon atoms. The wide-scan XPS does not indicate the existence of carbon in the final P- MnO_2 . The XPS results in Fig. S3 (ESI[†]) show that the spin-energy separation of 11.8 eV for P- MnO_2 is in agreement with MnO_2 materials reported elsewhere, also confirming that MnO_2 was obtained.¹⁹ The thermogravimetric analysis (Fig. S5, ESI[†]) does not indicate weight loss in the range of $300\text{--}600^\circ\text{C}$, which is observed for PGM due to the oxidation of carbon. This further confirms full replication of carbon by MnO_2 in the final P- MnO_2 .

The as-prepared P- MnO_2 powders were mixed with Super P (a conductive carbon black) and PTFE and used as the working electrodes to evaluate their electrochemical performance in a 1 M Na_2SO_4 aqueous electrolyte with a three-electrode cell. Fig. 3a shows that the cyclic voltammograms (CV) of the P- MnO_2 electrodes show no obvious distortion from 5 to 200 mV s^{-1} , indicating excellent ion diffusion in the electrode, while the CV curve of the control MnO_2 sample (C- MnO_2) prepared by a co-precipitation method is seriously distorted even when the scan rate increases to 100 mV s^{-1} (see ESI[†] for details and Fig. S4a).

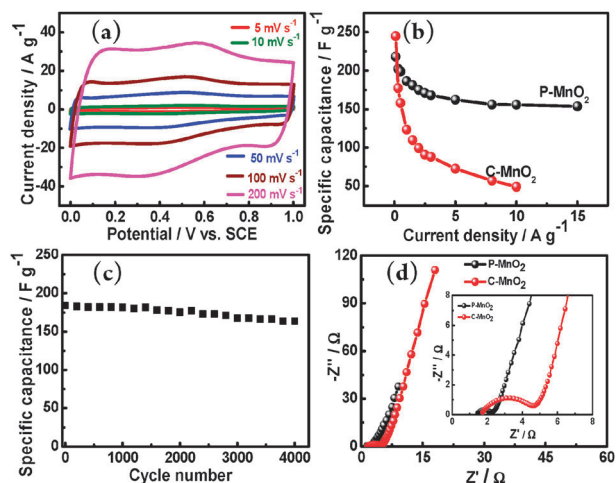


Fig. 3 (a) CV curves of P-MnO₂ at different scan rates. (b) Capacitance retention of P-MnO₂ and C-MnO₂ at different current densities. (c) Cycle performance of P-MnO₂ at a current density of 2 A g⁻¹. (d) Nyquist plots of P-MnO₂ and C-MnO₂.

In Fig. S4b (ESI[†]), a capacitance retention ratio as high as 72.8% is obtained at 200 mV s⁻¹, which is much higher than that of the control sample with a retention ratio of 31.2% at 200 mV s⁻¹ and other reported MnO₂ materials.²⁰

The results obtained from the constant current charge-discharge technique also prove that the novel P-MnO₂ material possesses high specific capacitance and superior power characteristics. As shown in Fig. 3b, the P-MnO₂ electrode exhibits a high capacitance of up to 218 F g⁻¹, and 70.6% of capacitance is retained even at a high current density of 15 A g⁻¹. In a sharp contrast, C-MnO₂ shows only 40.6% of capacitance retention at 2 A g⁻¹. In addition, the electrode displays promising cyclability. As shown in Fig. 3c, at a current density of 2 A g⁻¹, P-MnO₂ retains 90% of its original capacitance after 4000 cycles, indicating the excellent structural stability of the unique structure of this P-MnO₂ during the charge-discharge process, which is favourable for practical applications.

The excellent electrochemical properties of the P-MnO₂ material must be related to their unique structure and large specific surface area. First, porous MnO₂ provides a large accessible surface area to electrolyte ions for a fast surface sorption reaction. Second, the 3D framework and abundant mesopores of P-MnO₂ shorten the ion diffusion distance to the electrode and minimize the ion transfer resistance, which are synergistically beneficial for high rate performance. As shown in Fig. 3d, the charge transfer resistance of P-MnO₂ is as low as 0.9 Ω. Third, the large interlayer spacing of P-MnO₂ (about 0.7 nm)^{21,22} facilitates insertion of protons or cations in the electrode to accelerate the bulk redox reaction and contributes to the high pseudocapacitance.

In conclusion, this communication presents a simple but effective strategy for preparing nanoporous materials with a 3D interconnected channel replicating the nanostructure of the

graphene oxide hydrogel. In this strategy, the graphene oxide hydrogel with a 3D framework is used as a reactive and sacrificial template, and due to the thin-layered structure, almost all the carbon atoms can be replicated to form the produced porous materials. The produced materials can be separated from the reaction system and soluble reaction byproducts by a simple centrifugation, free of a complicated post-treatment. As an example for this strategy, nanoporous MnO₂ is produced in this study and shows great potential application in the field of supercapacitors. Its unique structure offering unimpeded ion diffusion channels endows P-MnO₂ with outstanding rate capability. Efforts are being made to replicate the 3D framework to functionalized materials and correlate the properties and the replicated structure.

This work was partially supported by the National Basic Research Program of China (2014CB932403), National Science Foundation of China (No. 51072131), State Key Laboratory of Heavy Oil Processing, NSF of Tianjin, China (No. 12JCZDJC27400) and Shenzhen Basic Research Project (Nos. JC201104210152A and JCYJ20130402145002430).

Notes and references

- 1 C. Largeot, C. Portet, J. Chmiola, P.-L. Taberna, Y. Gogotsi and P. Simon, *J. Am. Chem. Soc.*, 2008, **130**, 2730–2731.
- 2 F. Xu, R. Cai, Q. Zeng, C. Zou, D. Wu, F. Li, X. Lu, Y. Liang and R. Fu, *J. Mater. Chem.*, 2011, **21**, 1970–1976.
- 3 X. Maowen, K. Lingbin, Z. Wenjia and L. Hulin, *J. Phys. Chem. C*, 2007, **111**, 19141–19147.
- 4 J. P. Zheng, P. J. Cygan and T. R. Jow, *J. Electrochem. Soc.*, 1995, **142**, 2699–2703.
- 5 J. W. Lang, L. B. Kong, W. J. Wu, Y. C. Luo and L. Kang, *Chem. Commun.*, 2008, 4213–4215.
- 6 H. Itoi, H. Nishihara, T. Kogure and T. Kyotani, *J. Am. Chem. Soc.*, 2011, **133**, 1165–1167.
- 7 A. Kajdos, A. Kvit, F. Jones, J. Jagiello and G. Yushin, *J. Am. Chem. Soc.*, 2010, **132**, 3252–3253.
- 8 D.-W. Wang, F. Li, M. Liu, G. Q. Lu and H.-M. Cheng, *Angew. Chem., Int. Ed.*, 2008, **47**, 373–376.
- 9 P. Yu, X. Zhang, D. Wang, L. Wang and Y. Ma, *Cryst. Growth Des.*, 2008, **9**, 528–533.
- 10 D. L. Yan, S. C. Li, G. S. Zhu, Z. M. Wang, H. R. Xu and A. B. Yu, *Mater. Lett.*, 2013, **95**, 164–167.
- 11 X. Tang, Z.-h. Liu, C. Zhang, Z. Yang and Z. Wang, *J. Power Sources*, 2009, **193**, 939–943.
- 12 H. Nishihara and T. Kyotani, *Adv. Mater.*, 2012, **24**, 4473–4498.
- 13 C. O. Ania, V. Khomenko, E. Raymundo-Piñero, J. B. Parra and F. Béguin, *Adv. Funct. Mater.*, 2007, **17**, 1828–1836.
- 14 Y. Xu, K. X. Sheng, C. Li and G. Q. Shi, *ACS Nano*, 2010, **4**, 4324–4330.
- 15 W. Lv, Y. Tao, W. Ni, Z. Zhou, F.-Y. Su, X.-C. Chen, F.-M. Jin and Q.-H. Yang, *J. Mater. Chem.*, 2011, **21**, 12352–12357.
- 16 S. Chen, J. Zhu and X. Wang, *ACS Nano*, 2010, **4**, 6212–6218.
- 17 H. Huajie and W. Xin, *Nanoscale*, 2011, **3**, 3185–3191.
- 18 T. Gao, M. Glerup, F. Krumeich, R. Nesper, H. Fjellvåg and P. Norby, *J. Phys. Chem. C*, 2008, **112**, 13134–13140.
- 19 Z. Li, Y. Mi, X. Liu, S. Liu, S. Yang and J. Wang, *J. Mater. Chem.*, 2011, **21**, 14706–14711.
- 20 V. Subramanian, H. Zhu and B. Wei, *J. Power Sources*, 2006, **159**, 361–364.
- 21 Y. Ma, J. Luo and S. L. Suib, *Chem. Mater.*, 1999, **11**, 1972–1979.
- 22 S.-B. Ma, K.-Y. Ahn, E.-S. Lee, K.-H. Oh and K.-B. Kim, *Carbon*, 2007, **45**, 375–382.